Third AO4ELT Conference - Adaptive Optics for Extremely Large Telescopes
Florence, Italy. May 2013
ISBN: 978-88-908876-0-4
DOI: 10.12839/AO4ELT3.13297

MULTISCALE MODELING FOR THE SIMULATION OF NOT COMPLETELY FROZEN FLOW TURBULENCE

Alessandro Beghi[1], Angelo Cenedese[1], and Andrea Masiero[2a]

[1] University of Padova, Dipartimento di Ingegneria dell'Informazione, via Gradenigo 6/B, 35131 Padova, Italy
[2] University of Padova, CIRGEO, via dell'Università 16, 35020 Legnaro (PD), Italy

Abstract. Models typically used to simulate the influence of atmospheric turbulence on ground telescope observations are usually based on the frozen flow hypothesis. However, the frozen flow model of the atmosphere is valid at time scales of the order of tens/hundreds of milliseconds. This paper generalizes a previous model for turbulence simulation to ensure reliable tests of AO system performance in realistic working conditions. The proposed method relies on the use of a multiscale autoregressive-moving average model, which allows to efficiently simulate (with computational complexity $O(n)$) the coherent evolution of the turbulence. The proposed procedure is tested on simulations.

1 Introduction

High working frequencies, large dimension of the system (deformable mirrors of large telescopes are actuated by thousands of piezosystems), modeling uncertainties and nonlinearities make the goal of the control unit in AO systems quite challenging [1–8]. These considerations motivate an accurate testing procedure to compare different control strategies and evaluate their performance. According with this aim, this paper deals with the problem of statistically accurate simulation of the effect of atmospheric turbulence on ground telescope measurements.

Among the models previously proposed in the literature for the generation of turbulent phase screen, it is possible to distinguish models based on the use of the fast Fourier transform (FFT) [9], and methods based on linear dynamic systems [10–12]. The first are attractive because of their high accuracy, however their memory and computational requirements for long simulations are prohibitive. Then, much of the interest in the latter is due to their ability in producing long, possibly infinite, sequences of phase screens. Unfortunately, the computational complexity of methods [10–12] increases (approximately) quadratically with the turbulence resolution along one spatial direction. Thus, they cannot be used when dealing with both long exposure and high resolution simulations.

This work considers a generalization of the multiscale stochastic model for turbulence simulation proposed in [13]: this method, that has some analogies with other works in the literature concerning multiscale stochastic models [14–16], has the advantage that it allows the synthesis of long and accurate high resolution turbulent phase sequences with acceptable computational and memory requirements, i.e. O(n).

The proposed method, that is based on the use of a PCA local representation in combination with a multiscale stochastic model, can be extended to allow the simulation of nonstationary turbulence as well [17].

[a] masiero@dei.unipd.it

2 Turbulent phase characterization

From a spatial point of view, the turbulent phase is assumed to be zero-mean stationary and spatially homogeneous, and normally distributed [18]. Let $\mathbf{u}$ and $\mathbf{v}$ be two unit vectors indicating two orthogonal spatial directions, and let $\phi(u, v, t)$ be the value of the turbulent phase on the point (u, v) at time t on the telescope aperture plane, where u and v are the coordinates of the point along $\mathbf{u}$ and $\mathbf{v}$. Then, the covariance between two values of the turbulence, $\phi(u, v, t)$ and $\phi(u', v', t)$, depends only on the distance, r, between the two points: $C_\phi(r) = \mathbf{E}[\phi(u, v, t)\phi(u', v', t)], \forall (u, v, u', v')$, such that $r = \sqrt{(u - u')^2 + (v - v')^2}$.

According to the Von Karman theory, the shape of the spatial covariance function, $C_\phi(\cdot)$, is completely characterized by the values of two physical parameters, r_0, the Fried parameter, and L_0, the outer scale ([1, 19]):

$$C_\phi(r) = \left(\frac{L_0}{r_0}\right)^{5/3} \frac{\eta}{2} \left(\frac{2\pi r}{L_0}\right)^{5/6} K_{5/6}\left(\frac{2\pi r}{L_0}\right), \tag{1}$$

where $K_\cdot(\cdot)$ is the MacDonald function (modified Bessel function of the third type), and η is a constant [1, 19, 13].

From a temporal point of view, the turbulence is typically modeled as the superposition of a finite number ℓ of independent layers, moving at different altitudes, with different energies and velocities. Let $\psi_i(u, v, t)$ be the value of the i^{th} layer at point (u, v) and time t: the i^{th} layer models the atmosphere from h_{i-1} to h_i meter high, where $h_l \geq \cdots \geq h_i \geq h_{i-1} \geq \cdots \geq h_0 = 0$. Then, $\phi(u, v, t)$ is given by

$$\phi(u, v, t) = \sum_{i=1}^{\ell} \gamma_i \psi_i(u, v, t) \,, \tag{2}$$

where $\{\gamma_i\}$ are suitable normalized coefficients, i.e. $\sum_{i=1}^{l} \gamma_i^2 = 1$. The coefficients $\{\gamma_i^2\}$ have the physical meaning of strengths (or normalized energies) of the layers.

The layers are assumed to be characterized by similar spatial characteristics, i.e. all the layers are spatially described by the same covariance function $C_\psi(r)$:

$$C_\psi(r) = \mathbf{E}[\psi_i(u, v, t)\psi_i(u', v', t)] = C_\phi(r) \,, \; i = 1, \ldots, \ell \,, \tag{3}$$

where $r = \sqrt{(u - u')^2 + (v - v')^2}$.

A commonly agreed assumption (frozen flow hypothesis [1, 17]) considers that each layer translates in front of the telescope pupil with constant velocity $\boldsymbol{v}_i = v_{i,\mathbf{u}}\mathbf{u} + v_{i,\mathbf{v}}\mathbf{v}$:

$$\psi_i(u, v, t + k/f_s) = \psi_i(u - v_{i,\mathbf{u}} k/f_s, v - v_{i,\mathbf{v}} k/f_s, t) \,, \tag{4}$$

where f_s is the sampling rate, and k/f_s is a delay multiple of $1/f_s$.

In the simulation of stationary turbulent phase, in Section 5, the frozen flow hypothesis of Eq. 4 is assumed to hold. In addition, r_0 and L_0 are fixed to constant values.

However, the behavior of the real turbulence actually deviates from that established by the frozen flow approximation of Eq. 4: in order to take into account of such deviations, in the nonstationary case considered in Section 5.4, r_0 and L_0 are allowed to be time varying, as well.

Thanks to the independence of the layers, they can be simulated separately and then combined by means of Eq. 2. Without loss of generality, hereafter the paper takes into consideration the problem of simulating a single turbulent layer with velocity $\boldsymbol{v}(t) = v_{\mathbf{u}}(t)\mathbf{u} + v_{\mathbf{v}}(t)\mathbf{v}$, and strength $\gamma_1^2 = 1$.

3 Turbulent phase simulation

Consider a turbulent phase screen of size $r \times c$, where the physical dimension of each pixel in the corresponding matrix is $p_s \times p_s$. Then, the temporal turbulence evolution is equivalent to generating new rows and columns of the phase screen matrix and properly shifting the window corresponding to the telescope aperture of $(v_{\mathbf{v}}(t)/f_s, v_{\mathbf{u}}(t)/f_s)$ pixels at each sampling period[1] (see Fig. 1). Hence, the problem of simulating the temporal turbulence evolution can be reduced to that of generating a phase screen of larger size: to simplify the notation, hereafter we omit the time coordinate t from equations, and focus on the goal of generating an $r \times c$ phase screen.

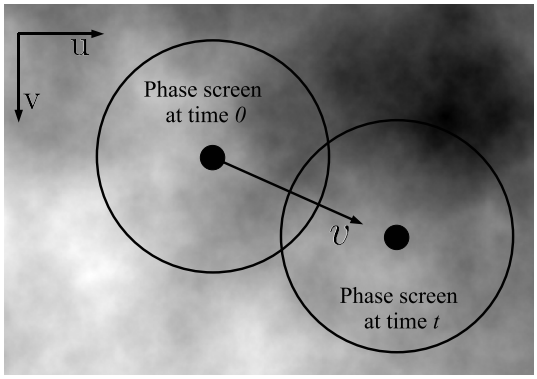

Fig. 1: Temporal evolution of the turbulence is obtained by generating new rows and columns of the phase screen matrix and shifting of $\boldsymbol{v}/f_s$) pixels the window corresponding to the telescope aperture.

4 Multiscale spatial representation based on local PCA

In this work, a multiscale representation of the turbulent phase is obtained by means of a local PCA decomposition.

Let l be the order of the representation level (l larger for scales associated to higher resolution, e.g. $M > 0$ is the scale associated to the highest resolution, whereas $l = 0$ is the lowest resolution scale), then define $x_M(u, v) = \phi(up_s, vp_s)$, $\forall (u, v) \in \mathbb{Z}^2$, where, with a slight abuse of notation, u and v are two spatial integer indexes.

The coefficients characterizing the turbulence at the spatial position (u, v) at scale $l - 1$ (e.g. $x_{l-1}(u, v)$) are obtained from those at scale l (e.g. $x_l(2u, 2v)$) by means of a local PCA decomposition. Consider the values of x_l in a proper 2×2 pixel spatial neighborhood of $(2u, 2v)$. The PCA representation of such pixels is given by the values of $\left[x_{l-1}(u, v)\ x_{l-1,1}(u, v)\ x_{l-1,2}(u, v)\ x_{l-1,3}(u, v) \right]^{\mathsf{T}}$:

$$\begin{bmatrix} x_l(2u, 2v) \\ x_l(2u, 2v+1) \\ x_l(2u+1, 2v) \\ x_l(2u+1, 2v+1) \end{bmatrix} = U_l S_l V_l(u, v) = U_l \begin{bmatrix} x_{l-1}(u, v) \\ x_{l-1,1}(u, v) \\ x_{l-1,2}(u, v) \\ x_{l-1,3}(u, v) \end{bmatrix}, \tag{5}$$

[1] For high accuracy simulations, $v_{\mathbf{v}}/f_s$ and $v_{\mathbf{u}}/f_s$ are restricted to be integer multiples of p_s.

where U_l is the 4×4 unitary matrix containing the spatial PCA bases[2], S_l is a diagonal matrix of singular values $(\sigma_{l,1}, \sigma_{l,2}, \sigma_{l,3}, \sigma_{l,4})$ in descending order, and $V_l(u, v)$ is a unit vector. x_{l-1} is a low pass representation of the turbulent phase, while $x_{l-1,1}$, $x_{l-1,2}$ and $x_{l-1,3}$ provide the spatial details to obtain x_l from x_{l-1}.

Recursively applying Eq. 5, the values of x_{l-1} are used to obtain the values of the representation at scale $l - 2$, and so on. Notice that at each scale the 2D domain is bisected in both directions with respect to the representation at the previous resolution level.

Since U_l is unitary, then Eq. 5 can be inverted by using $U_l^\top = U_l^{-1}$: by recursively using such linear relation, $\{x_l, x_{l,1}, x_{l,2}, x_{l,3}, \dots\}$ can be linearly expressed in terms of x_M, and vice versa.

When l is sufficiently large the last component of the PCA representation of Eq. 5 has typically much lower energy with respect to the others (i.e. $\sigma_{l,4} \ll \sigma_{l,3} \leq \sigma_{l,2} \leq \sigma_{l,1}$): as shown in the example of Fig. 2, typically $\sigma^2_{l,4}$, the energy of $x_{l-1,3}$, is usually much larger at the first scales than at the highest resolution ones. This suggests that in such a case $x_{l-1,3}$ can be neglected without affecting the statistical accuracy of the turbulence representation: in practical applications, a good tradeoff between statistical accuracy and computational time reduction is to neglect $x_{l-1,3}$ at the two highest resolution scales. Thus, the PCA representation can be exploited to reduce the number of values describing the current turbulent phase, and, consequently, the simulation time.

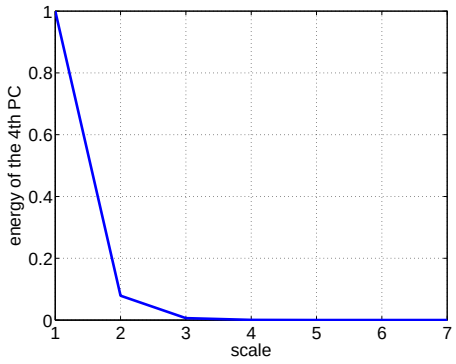

Fig. 2: Energy $\sigma^2_{l,4}$ of the 4th component in the multiscale PCA representation varying the scale l from 1 to $M = 7$. Turbulence parameters: $r_0 = 0.11$ m, $L_0 = 60$ m, $p_s = 8.2$ mm.

In order to take into account of the $x_{l-1,3}$ components neglected in the PCA representation at certain scales, Eq. 5 is modified as follows:

$$\begin{bmatrix} x_l(2u, 2v) \\ x_l(2u, 2v+1) \\ x_l(2u+1, 2v) \\ x_l(2u+1, 2v+1) \end{bmatrix} \simeq C_l \begin{bmatrix} x_{l-1}(u, v) \\ x_{l-1,1}(u, v) \\ x_{l-1,2}(u, v) \\ x_{l-1,3}(u, v) \end{bmatrix}. \tag{6}$$

where $C_l = \begin{bmatrix} U_l(:, 1:3) & \begin{matrix} 0 \\ 0 \\ 0 \\ 0 \end{matrix} \end{bmatrix}$ if $x_{l-1,3}$ is neglected, whereas $C_l = U_l$ otherwise.

[2] Since $x_M(u, v) = \phi(u, v)$, $\forall (u, v)$, and for each l the coefficients representing the turbulence at scale $l - 1$ can be linearly obtained from those at scale l, then the second order statistics of x_l can be obtained by means of linear combinations of values from Eq. 1.

5 Multiscale simulation of turbulence

The turbulent phase synthesis procedure can be summarized as follows:

- Use a low-resolution stochastic model to generate x_0, the turbulence at the lowest resolution, matching the second order statistics computed from Eq. 1.
- For each l, $0 \leq l < M-1$, use a proper stochastic model that takes as input x_l and provides as output a realization of x_{l+1}, that matches the theoretical second order statistics computed from Eq. 1.

The following subsections present the low-resolution and the multiscale stochastic models that allow to successfully perform the above steps. For simplicity of exposition, the border effect is discarded, i.e. at each scale the domain of the process is assumed to be an infinite grid. The reader is referred to [20] for a more detailed description of this aspect.

5.1 Lowest level MA model

x_0 is modeled as a spatial MA process, where the process x_0 at point (u, v) is obtained as a linear combination of the values of the random process ϵ_0 in a spatial neighborhood of (u, v):

$$x_0(u,v) = \sum_{k_u,k_v} \theta_0(k_u,k_v)\epsilon_0(u-k_u, v-k_v)\ , \tag{7}$$

where ϵ_0 is a zero-mean Gaussian white-noise process, and $\theta_0(\cdot,\cdot)$ are the coefficients of the MA process.

Since the turbulence covariance in Eq. 1 vanishes for large values of $r = \sqrt{u^2+v^2}$, then $C^0_\phi(u,v)$, the spatial covariance of x_0 evaluated at spatial distance (u, v), vanishes as well. Then, the sum in Eq. 7 can be practically thought as the sum of a finite number of terms: the range of values of indexes in the sum in Eq. 7 is assumed to be $k_u = -\delta_0, \ldots, \delta_0$, and $k_v = -\delta_0, \ldots, \delta_0$.

The computation of proper values of the parameters $\{\theta_0(\cdot)\}$ to make the covariances of the MA process match the theoretical ones can be solved in the (spatial) frequency domain (by using the fast Fourier Transform) as shown in [20].

Then, the simulation of the turbulence at the lowest resolution level is obtained by generating random numbers $\{\epsilon_0(u,v)\}$ and filtering them as in Eq. 7.

Since the generation of new portions of low resolution turbulence is made by using the local model of Eq. 7, which requires only that the underlying process ϵ_0 has been generated in the region of interest (and at its boundaries), then it allows to evolve the turbulence in spatial directions different from those of the axes **u** and **v**.

5.2 MAR–MA model for level l

In this paper the MAR–MA stochastic model proposed in [13] is used:

$$x_{l-1,1}(u,v) = \sum_{k_u,k_v} a_{l,k_u,k_v} x_l(u-k_u, v-k_v) + \sum_{k'_u,k'_v} \theta_l(k'_u,k'_v)\epsilon_{l,1}(u-k'_u, v-k'_v)\ , \quad \forall (u,v)\ , \tag{8}$$

where the coefficients $\{a_{l,k_u,k_v}\}$ allows a spatial prediction of the values of $x_{l-1,1}(u,v)$, given those of x_{l-1} in a spatial neighborhood of (u,v) (MAR process); the values of $\epsilon_{l,1}$ are randomly sampled from a zero-mean white-noise Gaussian distribution, and then are filtered using the coefficients

$\{\theta_l(k'_u, k'_v)\}$ (MA process, similar to that of the subsection 5.1). The range of values of k_u and k_v is $-d_l, \ldots, d_l$, while the range of k'_u, k'_v is $-\delta_l, \ldots, \delta_l$.

The MAR-MA stochastic models for $x_{l-1,2}$ and $x_{l-1,3}$ are similar to Eq. 8. According to Eq. 5, the model at level l, $l = \{1, \ldots, M\}$, takes x_{l-1} as input and aims at generating $x_{l-1,1}$, $x_{l-1,2}$ and $x_{l-1,3}$ such that the reconstructed x_l matches the theoretical statistics derived from Eq. 1 by means of linear operations: as shown in [13], the values of the parameters of the model (8) are computed in order to match the theoretical statistics of the stochastic process.

5.3 Synthesis procedure

The synthesis procedure can be summarized as follows (steps 5.A, 5.B, 5.C and 6 are performed only if the $x_{l,3}$ component is not neglected in the PCA representation):

1. MAR prediction of $x_{l,1}$ by using x_l as in Eq. 8,
2. Generate $\epsilon_{l,1}$ and filter it by means of the MA coefficients $\{\theta_{l,1}\}$ as in Eq. 8,
3. MAR prediction of $x_{l,2}$ by using x_l and $x_{l,1}$:
   3.A. Filter x_l with the corresponding coefficients in the MAR model for $x_{l,2}$,
   3.B. Filter $x_{l,1}$ with the corresponding coefficients in the MAR model for $x_{l,2}$,
4. Generate $\epsilon_{l,2}$ and filter it by means of the MA coefficients $\{\theta_{l,2}\}$,
5. MAR prediction of $x_{l,3}$ by using x_l, $x_{l,1}$ and $x_{l,2}$:
   5.A. Filter x_l with the corresponding coefficients in the MAR model for $x_{l,3}$,
   5.B. Filter $x_{l,1}$ with the corresponding coefficients in the MAR model for $x_{l,3}$,
   5.C. Filter $x_{l,2}$ with the corresponding coefficients in the MAR model for $x_{l,3}$,
6. Generate $\epsilon_{l,3}$ and filter it by means of the MA coefficients $\{\theta_{l,3}\}$,
7. Compute x_{l-1} by combining x_l, $x_{l,1}$, $x_{l,2}$, $x_{l,3}$.

5.4 Nonstationary turbulence

In practical applications, changes in the spatial characteristics of the turbulence (e.g. r_0, L_0) can occur, so, the parameters of the models (7) and (8) have to be changed accordingly. In this Section it is assumed that the turbulence characteristics can be thought as constant during (quite long) intervals, and they change abruptly from one set of values to another. So, actually, the turbulent phase can be simulated as a switching system.

It is simply to show that the parameters of the model (7) and (8) can be easily and quickly updated when only the value of r_0 changes: in such case, the new parameters can be computed by multiplying the previous values by multiplicative factors related to the new and old value of r_0.

Instead, when a change in the value of L_0 occurs, then the model parameters have to be recomputed following the complete procedure [13].

If needed, the evolution of r_0 and L_0 can be modeled as a Markov jump linear system, where L_0 varies among a predefined set of values (for which model parameters are precomputed offline).

Notice that spatio-temporal continuity of the generated turbulence has to be ensured when switching from one set of model parameters to another set [20].

6 Simulations and discussion

Fig. 3 compares the theoretical turbulence statistics with the sample ones estimated from phase screens (40 m × 20000 m) generated by means of: the complete MAR–MA model (the last component of the PCA representation is never discarded), the reduced complexity MAR–MA model previously suggested (the last component of the PCA representation is discarded at the two highest resolution scales, and at the highest resolution a reduced spatial neighborhood is considered in the MAR–MA), and the reduced complexity MAR–MA model where the last component of the PCA representation is discarded at all the scales.

Specifically, Fig. 3(a) compares the theoretical and the sample structure functions, whereas Fig. 3(b) compares the error on the sample structure functions with respect to the theoretical ones. Finally, Fig. 3(c) shows the difference between the structure functions obtained by the complete and the reduced complexity MAR–MA model.

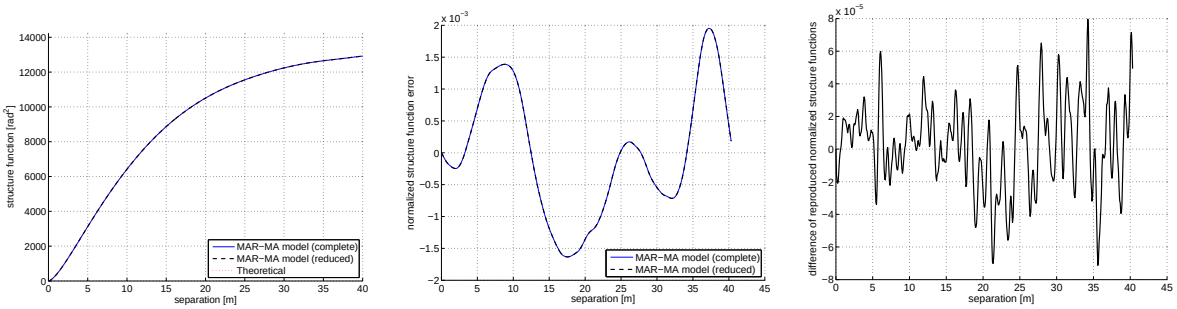

(a) (b) (c)

Fig. 3: (a) Comparison of the theoretical structure function (red dotted line) with the sample structure function obtained by means of the complete MAR–MA model (blue solid line), and the reduced complexity MAR–MA (black dashed line), estimated from a 40 m × 20000 m phase screen. (b) Error with respect to the theoretical structure function. (c) Difference between the structure functions obtained by the complete and the reduced complexity MAR–MA model. Turbulence parameters: $r_0 = 0.07$m, $L_0 = 60$m.

As expected, simulations confirm that the proposed use of local PCA allows a computational time reduction of approximately 73%. Furthermore, the reduced complexity (with the last component of the PCA representation discarded at the two highest resolution scales) and the full model provide practically equivalent results (Fig. 3(c)). The sample structure function estimated by synthesized data is very close to the theoretical one, while the computational time of the reduced complexity model is approximately 1/4 of that of the complete model: thus, the proposed model allows a particularly relevant time reduction without compromising the statistical accuracy.

Furthermore, the synthesis procedure can take advantage of the low resolution model of subsection 5.1 to dynamically evolve the turbulence in whatever direction: while the low level model in [13] accurately reproduces the turbulence statistics only if the turbulent phase moves along either the **u** or the **v** direction, the local model proposed here removes such requirement (actually, to ensure a good statistical accuracy, it only requires that $v_{\mathbf{v}}/f_s$ and $v_{\mathbf{u}}/f_s$ are integer multiples of p_s).

References

1. F. Roddier, Adaptive optics in astronomy, Cambridge univ.press, 1999.
2. D. Wiberg, C. Max, D. Gavel, Geometric view of adaptive optics control, Journal of the Optical Society of America A 22 (5) (2005) 870–880.
3. E. Gendron, P. Léna, Astronomical adaptive optics. 1: Modal control optimization, Astronomy and Astrophysics 291 (1994) 337–347.
4. L. Poyneer, J. Véran, Predictive wavefront control for adaptive optics with arbitrary control loop delays, Journal of the Optical Society of America A 25 (7) (2008) 1486–1496.
5. C. Correia, H. Raynaud, C. Kulcsár, J. Conan, On the optimal reconstruction and control of adaptive optical systems with mirror dynamics, Journal of the Optical Society of America A 27 (2) (2010) 333–349.
6. C. Béchet, M. Tallon, I. Tallon-Bosc, É. Thiébaut, M. Le Louarn, R. Clare, Optimal reconstruction for closed-loop ground-layer adaptive optics with elongated spots, Journal of the Optical Society of America A 27 (11) (2010) A1–A8.
7. I. Shatokhina, A. Obereder, M. Rosensteiner, R. Ramlau, Preprocessed cumulative reconstructor with domain decomposition: a fast wavefront reconstruction method for pyramid wavefront sensor, Applied Optics 52 (12) (2013) 2640–2652.
8. C. de Visser, M. Verhaegen, Wavefront reconstruction in adaptive optics systems using nonlinear multivariate splines, Journal of the Optical Society of America A 30 (1) (2013) 82–95.
9. B. McGlamery, Computer simulation studies of compensation of turbulence degraded images, in: Proceedings of SPIE 74, 1976, pp. 225–233.
10. F. Assemat, R. Wilson, E. Gendron, Method for simulating infinitely long and non stationary phase screens with optimized memory storage, Optic express 14 (3) (2006) 988–999.
11. A. Beghi, A. Cenedese, A. Masiero, Stochastic realization approach to the efficient simulation of phase screens, Journal of the Optical Society of America A 25 (2) (2008) 515–525.
12. D. Fried, T. Clark, Extruding Kolmogorov-type phase screen ribbons, Journal of the Optical Society of America A 25 (2) (2008) 463–468.
13. A. Beghi, A. Cenedese, A. Masiero, Multiscale stochastic approach for phase screens synthesis, Applied Optics 50 (21) (2011) 4124–4133.
14. A. Benveniste, R. Nikoukhah, A. Willsky, Multiscale system theory, Circuits and Systems I: Fundamental Theory and Applications, IEEE Transactions on 41 (1) (1994) 2–15.
15. K. Daoudi, A. Frakt, A. Willsky, Multiscale autoregressive models and wavelets, Information Theory, IEEE Transactions on 45 (3) (1999) 828–845.
16. R. Lane, A. Glindemann, J. Dainty, Simulation of a Kolmogorov phase screen, Waves Random Media 2 (3) (1992) 209–224.
17. M. Schöck, E. Spillar, Method for a quantitative investigation of the frozen flow hypothesis, Applied Optics 17 (9) (2000) 1650–1658.
18. F. Roddier, The effects of atmospheric turbulence in optical astronomy, Progress in Optics 19 (1981) 281–376.
19. R. Conan, Modelisation des effets de l'echelle externe de coherence spatiale du front d'onde pour l'observation a haute resolution angulaire en astronomie, PhD thesis, Univ. Nice Sophia Antipolis, 2000.
20. A. Beghi, A. Cenedese, A. Masiero, Multiscale phase screens synthesis based on local PCA, accepted in Applied Optics.